Mathematical Modelling and Simulation of Blood Flow in the Human Ascending Aorta: An Analytical Approach

T.O. Ajayi*, O. Oludare, and E. W. Ogunkoya,
Department of Chemical Engineering, University of Lagos, Lagos state, Nigeria
*tajayi@unilag.edu.ng

Abstract
The pulsatile behaviour of blood flow through a healthy aorta was modelled using Navier-Stokes and continuity equations, while the nature of the aorta wall was accounted for by Hooke's law. The resulting balance equations were transformed by using Reynolds transport theorem, and the variables expressed in Fourier modes. Substitution resulted in just one equation expressed in terms of Bessel functions, and which required one characteristic independent variable, k, to be determined. This was obtained by using Wolfram Mathematica to solve the equation along with aorta wall and blood properties (obtained from literature). The characteristic k value used for the prediction of the pulsatile nature of the flow was obtained as 0.139983 + 0.0590188i. Simulated results with this k value showed variation in blood pressure, aorta expansion and elongation, for a healthy heart to be within typical ranges of 80 – 120 mmHg, and 0 – 4mm respectively. The wavelength and wave speed generated by the blood flow was determined as 14.0848m and 53.8626m/s respectively.

Keywords: *Aorta blood flow, Newtonian fluid, Reynolds Transport Theorem, Wall pressure.*

1.0 INTRODUCTION

THE human body's physiological systems: integumentary, musculoskeletal, respiratory, digestive, urinary, reproductive, circulatory, nervous, endocrine and the immune systems, all work together to keep the body in a state of equilibrium – homeostasis. The circulatory (aka cardiovascular) system, which consists of the heart, blood vessels and blood, is charged with the responsibility of transporting various substances (O_2, CO_2, nutrients, metabolic products, vitamins, electrolytes, etc.), the transport of heat (heating, cooling), signal transmission (hormones), and buffering as well as defense against foreign materials and microorganisms. This essential, life-sustaining blood, amounting to 4-4.5 L in women and 4.5-5 L in men of 70 kg body weight (Silbernagl and Despopoulos, 2009), is pumped through blood vessels to body tissues by the heart. Blood is composed of blood cells (red blood cells, white blood cells, leukocytes and platelets) which are small semisolid particles which increase the viscosity of blood and affect its behavior (Thomas and Summan, 2016). The aorta is the main artery conveying oxygenated blood from the left ventricle of the heart to the rest of the body, and consists of four parts: ascending aorta, aortic arch, descending aorta and abdominal aorta (Figure 1). It is a vessel of complex geometry in that it curves, has branches off it and tapers in some regions (Chandran, 1993), all these affect the flow pattern of blood through it, which in turn determines the state of health of the aorta.

In the last decade, cardiovascular diseases, have risen to become the number one leading cause of death across the globe (WHO, 2017; Seta *et al.,* 2017), and per the American Heart Association, diseases of the aorta (aneurysm, arteriosclerosis and atherosclerosis) account for up to 47,000 deaths each year (Epps, 2012). The development of a better understanding of blood flow through the aorta is therefore of major importance to the etiology, diagnosis and prognosis of aortic diseases.

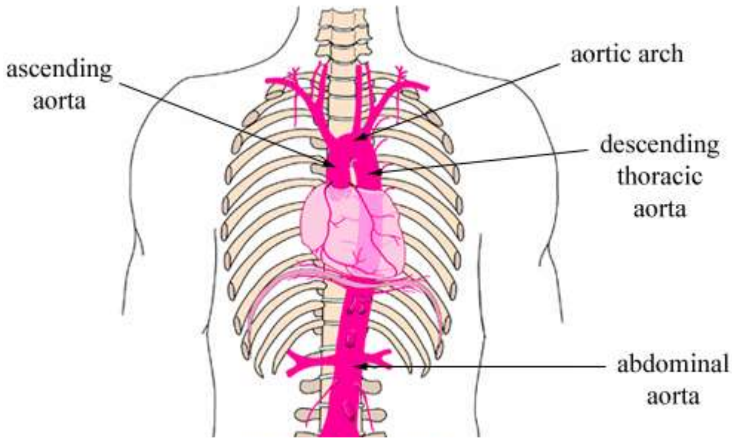

Figure 1: The Aorta (MedFriendly, 2012)

Generally, to gain better insights into physiological systems, there seems to be a paradigm shift in experimentations from *in vivo* and *in vitro* studies (qualitative analysis) to *in silico* studies (quantitative analysis), where mathematical models are used for computer simulation. In Valentinuzzi (2017) "*A statement reaches its maximum clarity and beauty when it can be expressed in mathematical terms*". Mathematical modelling of physiological systems is, therefore, about quantifying the qualitative using physical and engineering sciences to better understand and find solution to physiological problems.

2.0 METHODOLOGY

Using the laws of conservation, balance equations were obtained around an elemental aorta surface, the resulting equations were transformed by using Reynolds transport theorem, and the variables expressed in Fourier modes. Substitution method was then used to obtain the one model equation to be solved analytically.

2.1 BACKGROUND

Blood flow in the aorta is periodic in time, pulsatile, as shown in Figure 2b, the highest flowrate occurs when the left ventricle (see Figure 2a) pumps oxygenated blood into the aorta – the systole phase, and the low flowrate corresponds to when the aortic valve is closed and the venae cavae fills the right atrium with deoxygenated blood – the diastole phase. During this cardiac cycle the aorta deforms per the pressure exerted on it (Figure 2c), thus helping to regulate the blood flow in the body's circulatory system.

Most of the research works on the description of the behavior of blood flow and pressure in the systemic arteries commonly uses the Windkessel and other similar linear lumped models (Ursino, 1998; Leaning *et al*., 1983; Olufsen and Nadim, 2004; Catanho *et al*., 2012). A dimensionless parameter called Womersely number, α, is used to characterize the pulsatile nature of blood flow, and it is defined by $\alpha = a\sqrt{\frac{\omega}{\nu}}$, where *a* is the radius of the tube, ω is the frequency of the pulse wave (heart rate expressed in radians/sec) and ν is the kinematic viscosity of blood. The ability of the aorta wall vessel to expand and contrast passively with change in pressure is also an important feature.

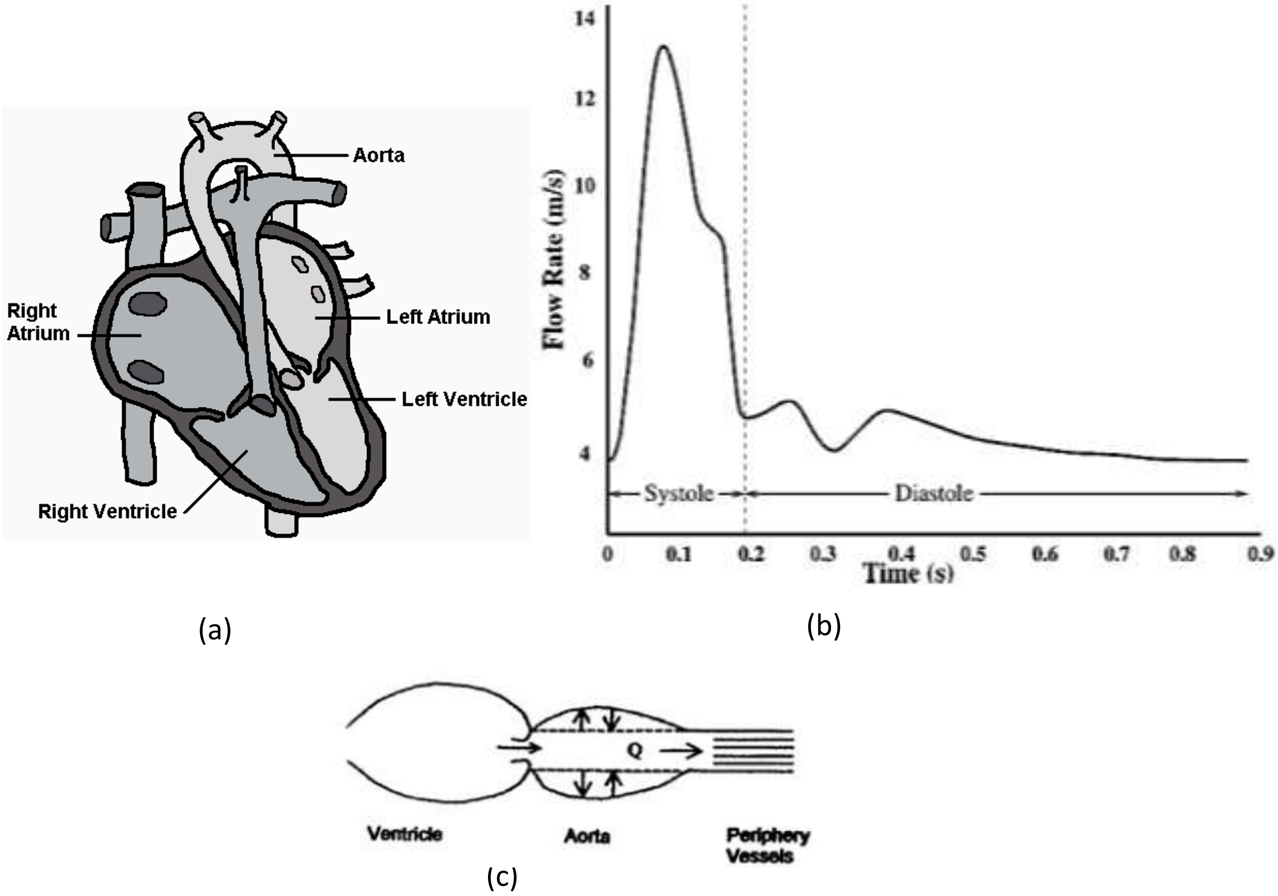

Figure 2: (a) The heart (Educational Designers, 2017); **(b)** A typical flowrate in the aorta during the systole-diastole cardiac cycle (Quarteroni and Formaggia, 2004); **(c)** Illustrating aorta deformation thus ensuring constant blood flow (Catanho *et al*., 2012)

2.2 STEADY BLOOD FLOW THEORY

Blood flow in a vessel is normally modeled as an incompressible, laminar flow fluid of a Newtonian nature through a straight, rigid, cylindrical tube of constant cross-sectional area. This type of flow is called circular Poiseuille flow or more commonly known as Hagen-Poiseuille flow.

Using the Hagen-Poiseuille model (Kundu *et al*., 2012), illustrated in Figure 3, and in cylindrical coordinates (r, θ, x) where x is the axial coordinate, r is the radial distance from the x-axis, P is pressure, and θ the circumferential angle. The axial flow velocity, $u = u(r)$

$$u(r) = \frac{r^2 - a^2}{4\mu}\left(\frac{dP}{dx}\right) \tag{1}$$

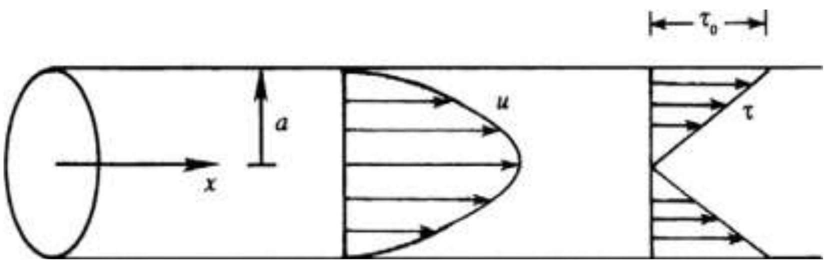

Figure 3: Hagen-Poiseuille Flow (Kundu, 2012)

2.3 ELASTICITY OF THE AORTA AND THE WINDKESSEL THEORY

During blood circulation in the body, it is not all the blood pumped into the aorta that goes into the systemic circulation. A part of the blood is used to distend the aorta and a part of the blood is sent to peripheral vessels. The distended aorta acts as an elastic reservoir or a Windkessel (Nico *et al*., 2009)

In the Windkessel theory, blood at the rate *Q(t)* from the left ventricle enters an elastic chamber (aorta) and a part of this flow out into a single rigid tube representative of all the peripheral vessels. The rigid tube offers constant resistance R, equal to the total peripheral resistance that was evaluated in the Hagen-Poiseuille model.

2.4 MODEL DEVELOPMENT

Most of the available proposed models on blood flow through the cardiovascular system are classified based on their dimensionality which ranges from zero dimensions (0-D) to three dimensions (3-D). In the 0-D model, also called lumped parameter models, it is assumed that the fundamental variables such as volume, pressure, density, flow etc. are uniformly distributed throughout the system at any point in time while the higher dimensions' model takes into cognizance the variations in these variables with respect to time and space.

3D numerical analysis, which is generally based on CT imaging (Morris *et al*., 2005), CFD (Benim *et al*., 2011; Caballero and Lain, 2015; Vinoth *et al*., 2017) and/or MRI imaging (Seta *et al*., 2017) provide real geometry and real flow conditions of blood flow in the aorta, but are complex and enormously computationally intensive (Grinberg *et al*., 2009; Rahman and Haque, 2012). In as much as these 3D simulations are invaluable to our understanding of most diseases, San and Staples (2012) noted that most facilities do not have ready access to these machines, there is therefore a need to have an approach that is less computationally intensive yet still accurate and can give useful results in a reasonable amount of time on a desktop computer. This paper obtains a model for blood flow in the ascending aorta that can be solved analytically without being cumbersome.

The Navier-Stokes and the continuity equations were used to develop a novel and simple one-dimensional equation, for blood flow in the ascending aorta.

The following simplifying assumptions, which have been defended in literature (Fairchild *et al*., 1966; Steinman 2012; Bessonov *et al.,* 2016; Vinoth *et al*., 2017), were used for developing the model:

(i) The ascending aorta is a straight tube with circular cross-section, and with a proximal (the part closest to the heart) diameter of 2-3 cm, and a distal diameter of 1 cm, in the human adult
(ii) The aorta wall is thin, elastic with material properties approximately homogeneous over the segment under consideration and obeys Hooke's law
(iii) Due to the comparatively large size of the aorta, blood flow is considered incompressible, homogeneous, Newtonian, and isotropic and temperature effect on blood properties is insignificant.
(iv) Flow is laminar with no secondary flow
(v) No chemical interaction with the aorta wall and diffusion through the aorta wall is negligible
(vi) Effect of temperature on blood properties is insignificant

Blood, which, is normally modelled as a non-Newtonian fluid, using the Casson or third grade fluid model, has been noted by many researchers (Bessonov *et al.,* 2016; Kundu *et al*., 2016; Vinoth *et al*., 2017; Seta and Vila ,2017; Menut *et al*., 2018) to behave like a Newtonian fluid in large arteries such as the aorta, where shear rate is greater than 100s^{-1}(Pedley, 2008). Considering blood as a Newtonian fluid, as is done in this paper, is therefore a satisfactory assumption for the aorta.

The objective of modelling is to determine the aorta wall stress as a function of the pressure and velocity of the blood flow, and this was achieved by taking mass, momentum, and force balances around the aorta, using the Reynolds transport theorem.

For any given intensive property, ϕ, Reynolds transport theorem (Albert, 2017) can be written as

$$\frac{d}{dt}\int_{W_{CM}} r f d\text{W}=\frac{\partial}{\partial t}\int_{W_{CV}} r f d\text{W}+\int_{S_{CV}} r f (v - v_b)\cdot n dS \tag{2}$$

where Ω_{CM} is the volume of the control mass, Ω_{CV} the volume of the control volume, S_{CV} the surface area enclosing the control volume, ρ is the density, $d\Omega$ the differential control volume of fluid, v the velocity of fluid flow, v_b is the reference velocity or the velocity with which control volume surface is moving, n the unit vector orthogonal to S_{CV} in the outward direction, ϕ is any given intensive property, and dS is the differential control surface area.

2.4.1 Mass Balance

Since the ascending aorta is stationary, and of a fixed control volume, $v_b = 0$ and for a mass balance, $\phi = \frac{m}{m} = 1$. Mass in the aorta is neither created nor destroyed within the system, thus equation (2) becomes

$$\frac{d}{dt}M\Big)_{system} = \frac{\partial}{\partial t}\int_{\Omega_{CV}} \rho d\Omega + \int_{S_{CV}} \rho v \cdot n dS = 0 \tag{3}$$

From Gauss-Ostrogradskii divergence theorem. (Bird *et al*., 2007; Wikipedia, 2017), $\int_{S_{CV}} (\rho v \cdot n) dS = \int_{\Omega_{CV}} (\nabla \cdot \rho v) d\Omega$ and equation (3) becomes

$$\int_{\Omega_{CV}} \left(\frac{\partial \rho}{\partial t} + \nabla \cdot \rho v\right) d\Omega = 0 \tag{4}$$

With the assumption that the aorta is a cylindrical tube with uniform cross section, density is constant and velocity and changes in θ-direction are negligible (where *r*, θ and *z* are cylindrical coordinates)

$$\frac{1}{r}\frac{\partial (r v_r)}{\partial r} + \frac{\partial v_z}{\partial z} = 0 \tag{5}$$

2.4.2 Momentum Balance

Considering only the *r* and *z* – directions of the cylindrical coordinate and assuming variations in θ-direction is negligible.

Conserved quantity is momentum *(mv)*, which implies $\phi = \frac{mv}{m}$ = *v*, Equation (2) gives

$$\frac{d}{dt}MV\Big)_{system} = \frac{\partial}{\partial t}\int_{\Omega_{CV}} (\rho v) d\Omega + \int_{S_{CV}} (\rho v v)\cdot n dS \tag{6}$$

where $\rho d\Omega = mass$ and $MV)_{system}$ = total momentum of the system. From Newton's second law of motion, $\frac{d}{dt}MV)_{system} = \sum F = \int_{\Omega_{CV}} b_i \rho d\Omega + \int_{S_{CV}} T \cdot n dS$ (Ferziger and Peric, 2002)

where: $F =$ Force, $b_i =$ Body force per unit mass, and $T =$ Surface force per unit area.
With body forces assumed negligible, applying the Gauss–Divergence theorem, differentiating and rewriting in the r – direction, gives

$$\nabla \cdot t_r = \frac{\partial \rho(v_r)}{\partial t} + \nabla \cdot (\rho v(v_r)) \tag{7}$$

where t_r represent surface forces in *r*-direction which is a function of force due to pressure, *P*, normal stress and tangential stresses. Therefore equation (7) can be written as:

$$\nabla \cdot t_r = -\frac{-\partial P}{\partial r} - \left[\frac{1}{r}\frac{\partial}{\partial r}(r\delta_{rr}) + \frac{1}{r}\frac{\partial}{\partial \theta}(\delta_{\theta r}) + \frac{\partial}{\partial z}(\delta_{zr}) - \frac{\delta_{\theta\theta}}{r} \right] \tag{8}$$

Combining equations (7) and (8), and introducing the same assumptions used for the mass balance, with negligible changes in the ϑ direction, only the *r* and *z* directions considered, that is $v_\theta = 0$, $\frac{\partial}{\partial \theta} = 0$ and substituting the Stoke's relations gives

$$\rho \frac{\partial v_r}{\partial t} = -\frac{\partial P}{\partial r} + \mu \left[\frac{\partial^2 v_r}{\partial r^2} + \frac{1}{r}\frac{\partial v_r}{\partial r} - \frac{v_r}{r^2} + \frac{\partial^2 v_r}{\partial z^2} \right] \tag{9}$$

$$\rho \frac{\partial v_z}{\partial t} = -\frac{\partial P}{\partial z} + \mu \left(\frac{\partial^2 v_z}{\partial r^2} + \frac{1}{r}\frac{\partial v_z}{\partial r} + \frac{\partial^2 v_z}{\partial z^2} \right) \tag{10}$$

2.4.3 Force Balances on the Aorta Wall

Let the aorta wall displacement in the *r*, θ and *z* directions be η, ς and ξ respectively. The density of the aorta wall material is given as ρ_w. The initial radius of the tube is a_0 and the thickness of the aorta wall is *h.* The aorta wall is assumed to obey Hooke's law and the bending stress during blood flow is negligible due to the thinness of the wall.
The circumferential tension of a thin elastic tube that obeys Hooke's law (Kundu, *et al*., 2012) is given as $T_\theta = \frac{Eh}{1-w^2}\left(\frac{\eta}{a_0} + w\frac{\partial \xi}{\partial z}\right)$ and the axial stress as $T_z = \frac{Eh}{1-w^2}\left(\frac{\partial \xi}{\partial z} + w\frac{\eta}{a_0}\right)$, where: T_θ = circumferential tension, T_z = axial stress, *E* = Young modulus constant and w = Poisson's ratio (ratio of the proportional decrease in thickness, lateral measurement, to the proportional increase in length of an elastic material that is stretched).
The Force balance is carried out on differential control volume of the aorta with the change in volume given as $d\Omega = hrd\theta dz$, τ_{rr} and τ_{rz} are stresses in the r- and z-directions respectively
In the r – direction,

$$\rho_w hrd\theta dz \frac{\partial^2 \eta}{\partial t^2} = \tau_{rr}\big|_{r=a} rd\theta dz - \frac{T_\theta}{a_0} rd\theta dz,$$

which gives

$$\rho_w h \frac{\partial^2 \eta}{\partial t^2} = \tau_{rr}\big|_{r=a} - \frac{T_\theta}{a_0}$$

$$\tau_{rr}\big|_{r=a} = P\big|_{r=a} - 2\mu\left(\frac{\partial v_r}{\partial r}\right)\bigg|_{r=a}$$

and

$$\rho_w h \frac{\partial^2 \eta}{\partial t^2} = P\big|_{r=a} - 2\mu\left(\frac{\partial v_r}{\partial r}\right)\bigg|_{r=a} - \frac{Eh}{1-w^2}\left(\frac{\eta}{a_0^2} + \frac{w}{a_0}\frac{\partial \xi}{\partial z}\right) \tag{11}$$

In the z –direction,

$$\rho_w h \frac{\partial^2 \xi}{\partial t^2} = -\mu\left(\frac{\partial v_z}{\partial r} + \frac{\partial v_r}{\partial z}\right)\bigg|_{r=a} + \frac{Eh}{1-w^2}\left(\frac{\partial^2 \xi}{\partial z^2} + \frac{w}{a_0}\frac{\partial \eta}{\partial z}\right) \tag{12}$$

Note, displacement in θ direction is also assumed to be negligible.

2.5 Analytical Solution of Equations

The equations that were derived to model blood flow through the aorta are given by Equations (5), (9), (10), (11) and (12) and these equations can be solved using either analytical or numerical methods. For the scope of this paper the analytical (substitution) method, is used.

2.5.1 Boundary Conditions:

The velocity component of the fluid at the wall is equal to the rate of elongation and expansion of the aorta. Therefore,

$$v_z\big|_{r=a_0} = \frac{\partial \xi}{\partial t}\bigg|_{r=a_0} \tag{13}$$

$$v_r\big|_{r=a_0} = \frac{\partial \eta}{\partial t}\bigg|_{r=a_0} \tag{14}$$

The five quantities or variables from the five equations obtained for the model can be represented in terms of Fourier modes because they are all periodic. Thus,

$$\left.\begin{aligned} v_r(z,r,t) &= \hat{v}_r(r)e^{i(kz-\omega t)} \\ v_z(z,r,t) &= \hat{v}_z(r)e^{i(kz-\omega t)} \\ P(z,t) &= \hat{P}\, e^{i(kz-\omega t)} \\ \eta(z,t) &= \hat{\eta}\, e^{i(kz-\omega t)} \\ \xi(z,t) &= \hat{\xi}\, e^{i(kz-\omega t)} \end{aligned}\right\} \tag{15}$$

where: $\hat{v}_r(r), \hat{v}_z(r), \hat{P}, \hat{\xi}, \hat{\eta}$ are amplitudes, $\omega = 2\pi/\overline{T}$ = Frequency of the forced disturbance, and $\overline{T}$ = Period of the heart cycle, k is a complex constant that defines the characteristics of the wave form and its given as $k = k_1 + ik_2$, where k_1 is wave number and k_2 is a damping constant which is a measure of decay of the disturbance as it moves along the aorta.

From (Kundu *et al.*, 2012), $2\pi/\lambda = |k| = \sqrt{k_1 + k_2}$, wavelength = $\lambda = \dfrac{2\pi}{|k|}$ and wave speed, $c = \dfrac{\omega}{k_1}$

Combining equations (15), (10) and (5), simplifying and since $\hat{v}_z(r)$ is only a function of radial coordinate, it can be expressed as

$$\frac{d^2 \hat{v}_z(r)}{dr^2} + \frac{1}{r}\frac{d\hat{v}_z(r)}{dr} + \frac{\rho \hat{v}_z(r) i\omega}{\mu} = \frac{\hat{p} ik}{\mu} \tag{16}$$

Equation (5) becomes

$$\frac{1}{r}\frac{d(r\hat{v}_r(r))}{dr} = -\hat{v}_z(r)ik \tag{17}$$

Rewriting equations (11) to (14) in terms of the Fourier modes of (15) and solving gives

$$\hat{P} = \frac{Eh}{a_0^2}\hat{\eta} - \frac{iw}{a_0 k}\mu\left.\frac{d\hat{v}_z(r)}{dr}\right|_{r=a_0} \tag{18}$$

$$\hat{\xi} = \frac{iw}{a_0 k}\hat{\eta} - \frac{1-w^2}{Ehk^2}\mu\left.\frac{d\hat{v}_z(r)}{dr}\right|_{r=a_0} \tag{19}$$

Substituting into equation (16) gives Bessel's differential equation

$$\frac{d^2\hat{v}_z(r)}{dr^2} + \frac{1}{r}\frac{d\hat{v}_z(r)}{dr} + \frac{\rho\hat{v}_z(r)i\omega}{\mu} = \frac{\hat{ik}}{\mu}\frac{Eh}{a_0^2}\hat{\eta} + \frac{w}{a_0}\mu\left.\frac{d\hat{v}_r(r)}{dr}\right|_{r=a_0},$$

whose solution is given as the Bessel function $\hat{v}_z(r) = AJ_0(\beta r) + \frac{k}{\omega}\frac{Eh}{\rho a_0^2}\hat{\eta} - \frac{w}{\beta a_0}AJ_1(\beta a_0)$

where $\beta = \sqrt{i\omega/\vartheta}$, *A* is arbitrary constant and ϑ is kinematic viscosity given as $\vartheta = \frac{\mu}{\rho}$

Solving equation (17) by substituting the Bessel function above with the given boundary conditions give:

$$\left(\frac{k^2}{\omega^2}\frac{Eh}{2\rho a_0}\right)^2\left[2\hat{\beta}\frac{J_0\left(\hat{\beta}\right)}{J_1\left(\hat{\beta}\right)} - 4\right] + \left(\frac{k^2}{\omega^2}\frac{Eh}{2\rho a_0}\right)\left[4w - 1 - 2\hat{\beta}\frac{J_0\left(\hat{\beta}\right)}{J_1\left(\hat{\beta}\right)}\right] + (1-w^2) = 0 \tag{20}$$

Simulation codes to solve Equation (20) were developed using Mathematica® along with the physiological data given in Table 1, to obtain an appropriate *k* value.

Table 1: Physiological data used in the simulation

Parameters	***Value***
Heartbeat per minute	72
Density of blood, ρ, kg/m^3	1050
Viscosity of blood, μ, kg/m/s	0.004
Diameter of aorta, d, m	0.025
Wall thickness of aorta, m	0.002
Poisson's ratio for aorta, υ	0.5
Young's Modulus of aorta, ε_i, Pascal	700,000

(Source: Morris *et al.*, 2005; *Benim et al.*, 2010)

3.0 RESULTS AND DISCUSSION

The *k* value obtained from equation (20) was then used in equation (15) to obtain pressure (*P*), elongation (*ξ*) and expansion (*η*) with respect to time. Using the pressure amplitude of 120mmHg as reference, the first *k* value (0.139983 + 0.0590188*i*) was chosen for the simulation because it gave the closest estimate of the predicted pressure amplitude (119.907mmHg) as compared to the value (119.522mmHg) obtained when the second *k* value (1.055640 + 0.0264822*i*) was used. The corresponding wavelength and wave speed of the chosen *k* value was obtained as 14.0848m and 53.8626m/s respectively. Figure 4 shows the resulting plot of blood pressure and elongation of the aorta with respect to time using both Re(*k*) and Im(*k*).

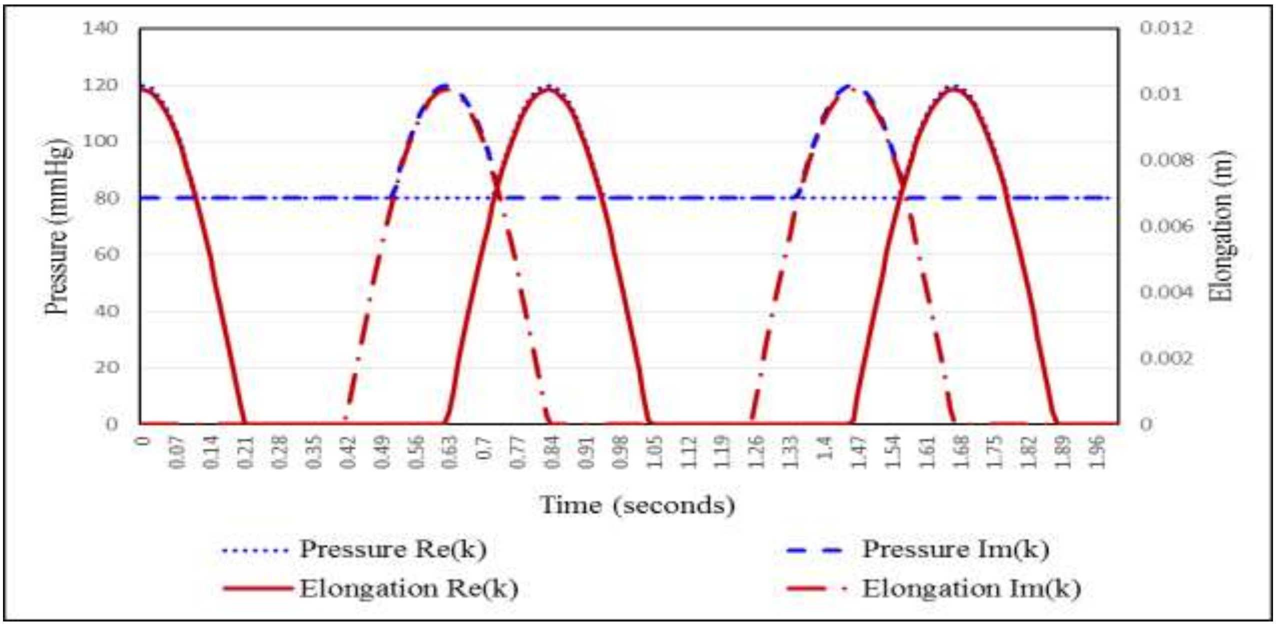

Figure 4: Plot of Pressure and Aorta Elongation against Time using Re(*k*) and Im(*k*)

In the simulation, it was assumed that the diastolic pressure in the aorta of a healthy adult is constant at 80mmHg while the systolic pressure rises from 80mmHg to 120mmHg during the systole phase of the cardiac cycle. This assumption was because there would be no blood flow in the aorta during the diastole phase of cardiac cycle because of the closure of pulmonary and aortic valves. Similarly, there would be no expansion and elongation of the aorta during this period. Hence, all pressure values below 80mmHg from the model simulations were normalized to 80mmHg while all expansion and elongation values below zero were also normalized to zero.
Re(*k*), resulted in sinusoidal waveforms while the use of Im(*k*), gave cosine waveforms of same wave characteristics for any fixed value of *z*. Figure 5 presents the pulsatile behaviour of blood pressure, aorta elongation and expansion for both real and imaginary parts of the *k* value.

The k value used for simulating the pulsatile behavior of blood flow showed variation in blood pressure, aorta expansion and elongation, for a healthy heart to be within typical ranges of 80 – 120 mmHg, and 0 – 4mm respectively. The wavelength and wave speed generated by the blood flow was determined as 14.0848m and 53.8626m/s respectively.

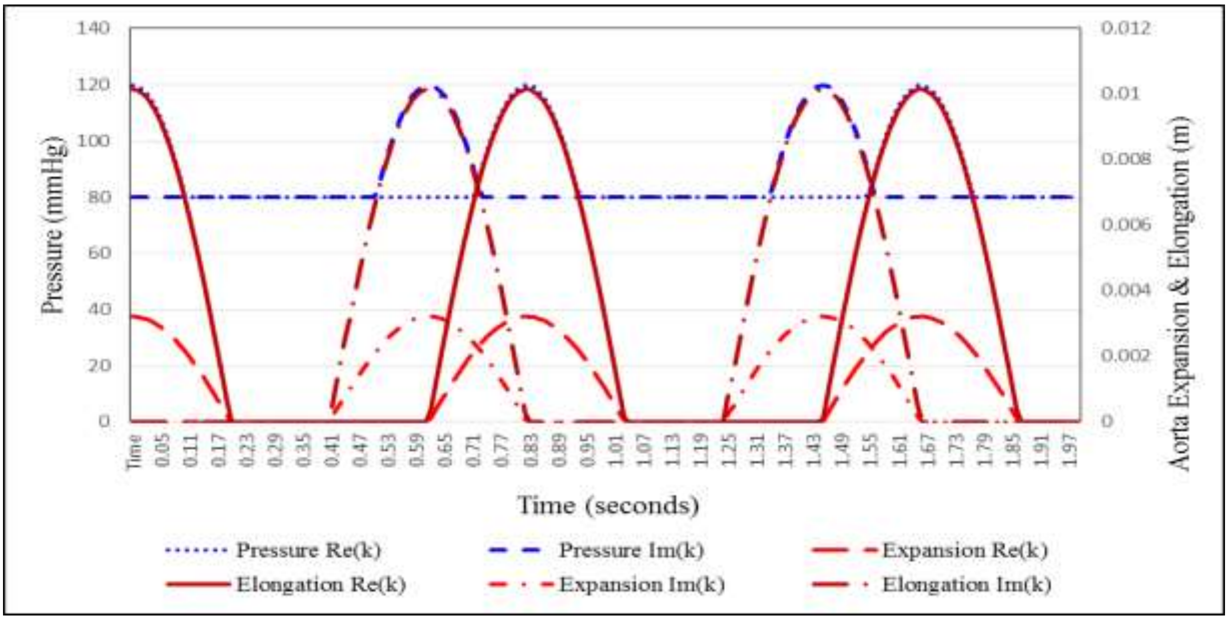

Figure 5: Plot of Pressure, Aorta Expansion and Elongation against Time using Re(k) and Im(k)

4. CONCLUSION

An analytical model was obtained for blood flow through the ascending aorta using Navier-Stokes and continuity equations. The resulting solution showed that for a given set of physiological data (mechanical properties of the aorta wall and blood properties), just one parameter, the k value, is required to predict the pulsatile behaviour (of pressure, elongation and expansion) of the blood flow through the aorta. However, because of the quadratic nature of the analytical model, two different k values were obtained, but the value that gave the closest approximation of the measured amplitudes was chosen.

REFERENCES

Albert, O. (2017). *Reynolds Transport Theorem*. distart119.ing.unibo.it/albertold/files/Reynoldstheorem.pdf, Acessed 3/7/17.

Benim, A. C., Nahavandi, A., Assmann, A., Schubert, D., Feindt, P. and Suh, S.H. (2011). Simulation of blood flow in human aorta with emphasis on outlet boundary conditions. *Applied Mathematical Modelling,* 35 (**7**): 3175-3188.

Bessonov, N., Sequeira, A., Simakov, S., Vassilevskii, Yu, and Volpert, V. (2016). Methods of Blood Flow Modelling. *Math. Model. Nat. Phenom*. 11(**1**): 1–25

Bird, B. R., Stewart, W. E., and Lightfoot, E. N. (2007). *Transport Phenomena* (2nd ed.). New York: John Wiley and Sons Inc., 731-732.

Caballero, A.D. and Lain,S.(2015). Numerical simulation of non-Newtonian blood flow dynamics in human thoracic aorta, *Computer Methods in Biomechanics and Biomedical Engineering*, 18 (**11**):200-1216.

Catanho M., Sinha M., and Vijayan V. (2012). Model of Aortic Blood Flow using the Windkessel Effect. BENG 221 - *Mathematical Methods in Bioengineering Report*, http://isn.ucsd.edu/classes/beng221/problems/2012/BENG221_Project-Catanho Sinha Vijayan.pdf, accessed 13/10/17

Chandran, K.B. (1993). Flow dynamics in the human aorta. *J. Biomech. Engng.* **115**: 611–616.

Educational Designers (2017) The human Heart, http://www.myschoolhouse.com/courses/O/1/94.asp, Accessed 1/11/17

Epps, R.F. (2012). *The Human Aorta: Your Super Highway of Life*, Gazelle Press, United States, 3-6

Fairchild, B. T., Krovetz, L. J., and Huckaba, C. E. (1966). Digital Computer Simulation of Arterial Blood Flow. In: Hershey, D. (Ed) *Chemical Engineering in Medicine and Biology*. Proceedings of the 33rd Annual Chemical Engineering Symposium of the Division of Industrial and Engineering Chemistry of the American Chemical Society, Held at the University of Cincinnati, on October 20-21, 1966. Plenum Press, New York. 3 – 43.

Ferziger, J. H., and M. Peric (2002). *Computational Methods for Fluid Dynamics* (3rd ed.), New York; Springer, 1 - 20
Grinberg, L., Anor, T., Madsen, J.R. Yakhot, A. and G.E. Karniadakis (2009). Large-scale simulation of the human arterial tree. *Clinical and Experimental Pharmacology and Physiology*, 36 (**2**):194 -205.
Hall, J.E. (2011). Guyton and Hall Textbook of Medical Physiology (12th Edition), Elsevier Inc., 177- 178
Kundu, P. K., Cohen, I. M., and Dowling, D. R. (2016). *Fluid Mechanics* (6th ed.). Oxford: Elsevier Inc., 779 -820, e11 - e20.
Leaning, M. S., Pullen, H. E., Carson, E. R., and Finkelstein, L. (1983). Modelling a Complex Biological System: The Human Cardiovascular System - 1. Methodology and Model Description. *Transactions on Institute of Measurement and Control,* 5 **(2**): 71–86.
MedFriendly. (2012). Aorta. http://medfriendly.com/aorta.html, Accessed 9/12/17
Menut M, Boussel L, Escriva X, Bou-Saïd B, Walter-Le Berre H, Marchesse Y, Millon A, Della Schiava N, Lermusiaux P, Tichy J. (2018). Comparison between a generalized Newtonian model and a network-type multi-scale model for hemodynamic behavior in the aortic arch: Validation with 4D MRI data for a case study. *Journal of Biomechanics* 73, 119–126
Morris, L., Delassus, P., Callanan, A., Walsh, M., Wallis, F., Grace, P. and T. McGloughlin (2005). 3-D numerical simulation of blood flow through models of the human. *J Biomech Eng*. Oct., 127 (**5**): 767-775.
Nico, W., Jan-Willem, K., and Berend, E. W. (2009). The Arterial Windkessel. *Med. Biol. Eng. Comput*. **47**: 131-141
Olufsen, M. S., and Nadim, A. (2004). On Deriving Lumped Models for Blood Flow and Pressure in The Systemic Arteries. *Mathematical Biosciences and Engineering,* 1(**1**), 61-80.
Quarteroni A. and Formaggia L., (2004). Computational Models for the Human Body. In Ayache N and P.G Ciarlet. (Eds) Handbook of Numerical Analysis*, Volume 12- Mathematical Modelling and Numerical Simulation of the Cardiovascular System*, 7 – 15
Pedley. T. J. (2008). The Fluid Mechanics of Large Blood Vessels Cambridge Monographs on Mechanics, Cambridge University Press.
Rahman, M. S. and Haque, M. A. (2012). Mathematical Modelling of Blood Flow. In *IEEE, International Conference on Informatics, Electronics and Vision, ICIEV*, Bangladesh, 672 - 676
San, O. and Staples A. E. (2012). An Improved Model for Reduced-Order Physiological Fluid Flows *J. Mech. Med. Biol.* 12, (**3**): 1-28
Seta B., Torlak M. and Vila A. (2017) Numerical Simulation of Blood Flow through the Aortic Arch. In: Badnjevic A. (Ed) *IFMBE Proceedings of the International Conference on Medical and Biological Engineering*. Springer, Singapore, **62**: 259-268
Silbernagl S. and Despopoulos A. (2009). *Color Atlas of Physiology*, 6th edition, Thieme, Stuggart. 88, 186, 190
Steinman D.A. (2012). Assumptions in modelling of large artery hemodynamics. In: Ambrosi D., Quarteroni A., Rozza G. (Eds) *Modeling of Physiological Flows— Modeling, Simulation and Applications*, Vol 5. Springer, Milano, 1 - 18
Thomas B. and K. S. Sumam (2016). Blood Flow in Human Arterial System - a Review. *Procedia Technology* **24**, 339 - 346.
Ursino, M. (1998). Interaction between Carotid Baroregulation and the Pulsating Heart: a Mathematical Model . *Am. J. Physiol.,* **275**, 1733 - 1747.
Valentinuzzi M. E and Arini P.D. (2017). Mathematical Models in bioengineering. In Valentinuzzi M. E (Ed) Further Understanding of the Human Machine - The Road to Bioengineering*, Series on Bioengineering and Biomedical Engineering: Volume 7, World Scientific, Singapore, pp 501 - 521*
Vinoth, R., Kumar, D., Raviraj, A., and Vijay S. (2017). Non-Newtonian and Newtonian blood flow in human aorta: A transient Analysis. *Biomedical Research*. 28 (**7**): 3194-3203
Wikipedia. (2017). *Divergence theorem*, https://en.wikipedia.org/wiki/Divergence_theorem Acessed 3/7/17
World Health Organization. (2017). *Cardiovascular Diseases*. http://www.who.int/mediacentre/factsheets/fs317/en/, Accessed 14/12/17

NOMENCLATURE

a_o initial radius of aorta,
a final radius of aorta
dS differential control surface area
E *Young* modulus constant
h thickness of aorta wall
$\kappa =$ Dilatational viscosity,
L length of tube
n unit vector orthogonal to S_{CV} in the outward direction,
P Pressure,
r axial distance from tube axis
r, θ and *z* are cylindrical coordinates
S_{CV} Surface area enclosing the control volume,
t time
T_θ circumferential tension, T_z axial stress,

v kinematic viscosity of blood
V velocity of fluid flow,
w Poisson's ratio of aorta
x tube axis,
α womersely number
$\delta_{rz}, \delta_{\theta z}, \delta_{zz}$ and $\delta_{\theta\theta} =$ Stress tensors.
η, ς and ξ are aorta wall displacement in the *r*, θ and *z* directions respectively
$\mu =$ blood viscosity,
ρ blood density, ρ_w density of aorta wall
ϕ any given intensive property,
ω frequency of pulse wave
Ω_{CM} Volume of the control mass,
Ω_{CV} Volume of the control volume,
$d\Omega$ differential control volume of fluid,
v_b reference velocity or the velocity with which control volume surface is moving,